Spectral and Conformational Analysis of Deoxyadenosine Adducts Derived from *syn*- and *anti*-Dibenzo[*a,l*]pyrene Diol Epoxides: Fluorescence Studies

Ryszard Jankowiak,*[,†] Cheng-Huang Lin,[‡] Dan Zamzow,[†] Kenneth P. Roberts,[†,‡] Kai-Ming Li,[§] and Gerald J. Small[†,‡]

Ames Laboratory-U.S. Department of Energy and Department of Chemistry, Iowa State University, Ames, Iowa 50011, and Eppley Institute for Research in Cancer and Allied Diseases, University of Nebraska Medical Center, 600 South 42nd Street, Omaha, Nebraska 68198

Received October 19, 1998

Low-temperature fluorescence spectra and results of conformational studies with *trans-syn*-, *cis-syn*-, *trans-anti*-, and *cis-anti*-dibenzo[*a,l*]pyrene diol epoxide (DB[*a,l*]PDE)-derived deoxyadenosine (dA) adducts are presented and compared with those previously obtained for the stereoisomeric DB[*a,l*]P tetrols [Jankowiak, R., et al. (1997) *Chem. Res. Toxicol.* **10**, 677−686]. In contrast to DB[*a,l*]P tetrols, for which only *trans* isomers exhibited two conformers, all stereoisomeric dA adducts adopt two different conformations with either half-chair or half-boat structures for the cyclohexenyl ring, and an "open"- or "folded"-type configuration between dA and the DB[*a,l*]P moiety. The major conformations observed for *trans-syn*-, *cis-syn*-, and *cis-anti*-DB[*a,l*]PDE−14-N^{6}dA could be assigned on the basis of the previous calculations for the DB[*a,l*]P tetrols. The major conformers of the *trans-syn*- and *cis-syn*-DB[*a,l*]PDE−14-N^6-dA adducts exist in conformations I and II, with their fluorescence origin bands at ∼382 and ∼389 nm, respectively. In conformation I, the cyclohexenyl ring adopts a half-boat structure with dA in a pseudoaxial position (an open configuration), whereas the cyclohexenyl ring in conformation II adopts a half-chair structure with dA in pseudoequatorial position (a folded configuration). The major conformation of *cis-anti*-DB[*a,l*]PDE−14-N^{6}dA, with its origin band at ∼389 nm, was also assigned as a folded-type configuration with a half-chair structure in the cyclohexenyl ring. Molecular mechanics and dynamical simulations were performed for interpretation of the low-temperature fluorescence spectra and ^{1}H NMR coupling constants observed for the *trans-anti*-DB[*a,l*]PDE−14-N^{6}dA adduct. The major conformer of this adduct has a half-chair structure in the cyclohexenyl ring, but a deviation from planarity in the fjord region different from that of conformer II of *cis-anti*-DB[*a,l*]PDE−N^{6}dA. This new structure is labeled as conformer II′. Its (0,0) fluorescence band is at 388.1 and 388.3 nm in ethanol and glycerol/water glasses, respectively, consistent with the folded-type configuration revealed by the calculations. The fluorescence line-narrowed spectra reveal that the *trans-syn*-, *cis-syn*-, *trans-anti*-, and *cis-anti*-DB[*a,l*]PDE−14-N^{6}dA adducts can be distinguished. Thus, their spectra should prove useful for identification of DB[*a,l*]P−DNA adducts formed at low levels in biological samples.

Introduction

Dibenzo[*a,l*]pyrene (DB[*a,l*]P)[1] is the most potent carcinogen among the polycyclic aromatic hydrocarbons (PAHs) (*1*, *2*). It has been found in river sediment (*3*) and indoor (*4*) and outdoor (*5*) air samples, suggesting potential (eco)toxicological hazards. DB[*a,l*]P can be enzymatically activated by two main pathways: one-electron oxidation to yield radical cations (*6*−*9*) and monooxygenation to produce bay-region diol epoxides (*10*−*15*). Numerous DB[*a,l*]P−DNA adducts have been reported (*6*−*16*).

Low-temperature fluorescence spectroscopy has proven to be a valuable tool for DNA adduct characterization. In particular, fluorescence line-narrowing spectroscopy (FLNS) (*8*, *17*) has been used for definitive identification (*6*, *8*−*24*) of adducts. Furthermore, the combination of FLNS and non-line-narrowing (NLN) fluorescence spectroscopy can provide adduct conformational information

* Corresponding author. E-mail: jankowiak@ameslab.gov.
† Ames Laboratory-U.S. Department of Energy, Iowa State University.
‡ Department of Chemistry, Iowa State University.
§ University of Nebraska Medical Center.

[1] Abbreviations: CE, capillary electrophoresis; dAMP, deoxyadenosine monophosphate; DB[*a,l*]P, dibenzo[*a,l*]pyrene; DB[*a,l*]PDE, dibenzo[*a,l*]pyrene diol epoxide; DB[*a,l*]PDE−14-N^2-dG, dibenzo[*a,l*]pyrene diol epoxide−N^2-deoxyguanosine; *syn*-DB[*a,l*]PDE−14-N^{6}dA, *syn*-dibenzo[*a,l*]pyrene diol epoxide−14-N^6-deoxyadenosine; *anti*-DB[*a,l*]-PDE−N^{6}dA, *anti*-dibenzo[*a,l*]pyrene diol epoxide−14-N^6-deoxyadenosine; DB[*a,l*]PDE−14-N7Ade, 14-(adenin-7-yl)-11,12,13-trihydroxy-11,-12,13,14-tetrahydrodibenzo[*a,l*]pyrene; DB[*a,l*]PDE−14-N7Gua, 14-(guanin-7-yl)-11,12,13-trihydroxy-11,12,13,14-tetrahydrodibenzo[*a,l*]-pyrene; DB[*a,l*]P tetrol, 11,12,13,14-tetrahydroxy-11,12,13,14-tetrahydrodibenzo[*a,l*]pyrene; DE, diol epoxide; FLNS, fluorescence line-narrowing spectroscopy; g/w, glycerol/water; MD, molecular dynamics; Me_2SO, dimethyl sulfoxide; MM, molecular mechanics; PAH, polycyclic aromatic hydrocarbon; S_0 state, electronic ground state; S_1 state, lowest excited singlet state; ZPL, zero-phonon lines.

10.1021/tx980233s CCC: $18.00
Published on Web 07/29/1999

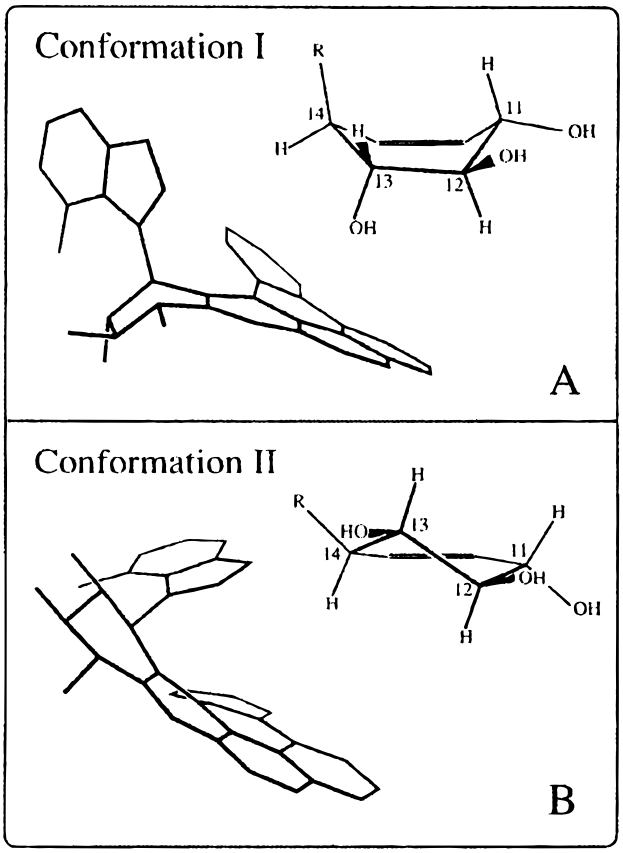

Figure 1. Optimized 0 K ground state structures of *trans-syn*-DB[*a*,*l*]PDE−14-N7Ade obtained after simulated annealing. Conformers I and II are shown in frames A and B, respectively. The insets show the conformation of the cyclohexenyl ring (half-boat vs half-chair); R is adenine. Hydrogens and double bonds were omitted for clarity. Results from ref *24*.

(*23*−*25*), i.e., whether the adduct is external, base-stacked, or intercalated. This methodology has recently been used to characterize DB[*a*,*l*]P diol epoxide (DB[*a*,*l*]-PDE)-derived DNA adducts and conformation-dependent DNA repair (*16*). These studies were performed using polynucleotides and calf thymus DNA reacted in vitro with DB[*a*,*l*]PDE and native DNA from mouse skin epidermis exposed to DB[*a*,*l*]P. It was shown that DB-[*a*,*l*]PDE−DNA adducts possess stereochemically different structures and can adopt different conformations (*16*). The results indicated a need for spectral characterization of all DB[*a*,*l*]PDE-derived deoxyadenosine (dA) adduct standards at the nucleoside level.

Fluorescence and computational studies have shown that *trans-syn*-DB[*a*,*l*]P tetrol (*26*) and the depurinating adduct *trans-syn*-DB[*a*,*l*]PDE−14-N7Ade (*24*) possess two distinct fluorescence (0,0) bands having different excited state vibrational frequencies. Molecular dynamics simulations (in vacuo) identified two conformers for the DB-[*a*,*l*]P tetrols and *trans-syn*-DB[*a*,*l*]PDE−14-N7Ade. The aromatic portion of DB[*a*,*l*]P was severely distorted, and half-chair or half-boat structures for the cyclohexenyl ring were observed (*24*, *26*). An example, relevant to the results of this paper, is shown in Figure 1. Two unique structures (conformers I and II) are shown for *trans-syn*-DB[*a*,*l*]PDE−14-N7Ade. In the open-type adduct structure (frame A), the cyclohexenyl ring adopts a half-boat structure where no significant interaction between the adenine (Ade) and the aromatic system is possible. In the folded-type conformation II (frame B), Ade is in a pseudoequatorial position and the cyclohexenyl ring adopts a half-chair structure. Similar conformations were observed for *trans-syn*-DB[*a*,*l*]P tetrol (*26*). The calculated and observed fluorescence origin bands established for various conformations of the *trans-syn-*, *cis-syn-*, *trans-anti-*, and *cis-anti*-DB[*a*,*l*]P tetrols, as well as the calculated dihedral angles and the estimated ^{1}H NMR coupling constants for the proton pairs of the cyclohexenyl ring, are summarized in Table 1. For stereoisomeric DB-[*a*,*l*]P tetrols, the agreement between the measured and theoretically estimated NMR coupling constants suggests that the results shown in Table 1 may be useful for interpretation of the spectroscopic data obtained for DB-[*a*,*l*]PDE−dA adducts.

In this work, DB[*a*,*l*]PDE−dA adducts, for which eight stereochemical configurations are shown in Figure 2, were studied by low-temperature fluorescence spectroscopy and molecular modeling. The NLN and FLN spectra of *trans-anti*, *cis-anti*, *trans-cis*, and *cis-syn*-DB[*a*,*l*]PDE−14-N⁶dA adducts presented below provide the necessary spectral information for investigating the nature of DB-[*a*,*l*]PDE−DNA adducts formed at low levels in in vitro and in vivo studies. The structural characterization of these adducts by NMR, circular dichroism, and fast atom bombardment mass spectrometry is presented elsewhere.[2]

Materials and Methods

Caution: *anti- and syn-DB[a,l]P diol epoxides are extremely hazardous chemicals and should be handled carefully in accordance with NIH guidelines.*

Sample Preparation. The DB[*a*,*l*]PDE-derived adducts *trans-anti-*, *cis-anti-*, *trans-syn-*, and *cis-syn*-DB[*a*,*l*]PDE−14-N⁶dA were synthesized by the reaction of *anti-* and *syn*-DB[*a*,*l*]-PDE with dA. The (±)-*anti*-DB[*a*,*l*]PDE was reacted with dA in dimethylformamide at 100 °C for 30 min to give four *anti*-DB-[*a*,*l*]PDE−14-N⁶dA adducts. The (±)-*syn*-DB[*a*,*l*]PDE was reacted with dA under the same conditions to yield the four *syn*-DB[*a*,*l*]PDE−14-N⁶dA adducts. For details on the synthesis and structural characterization, see the paper by K.-M. Li et al.[2]

Adduct Purity. The purity of dA standards separated by HPLC was checked by capillary electrophoresis (CE), which possesses higher separation power (i.e., higher efficiency) than HPLC. A mixture of 85% A [40 mM dioctyl sulfosuccinate and 8 mM sodium borate in 30% (by volume) acetonitrile/70% water (pH 9)] and 15% B (50 mM Brij S) was used as the CE buffer. These conditions allowed for separation of all eight diastereomers.[3] Figure 3 shows room-temperature absorbance electropherograms of HPLC-separated (−)-*trans-anti-* (a), (−)-*cis-anti-* (b), (+)-*trans-syn-* (c), and (+)-*cis-syn*-DB[*a*,*l*]PDE−14-N⁶dA (d). The results establish that the purity levels are very high, and thus, one can be confident that the library of NLN and FLN spectra that was obtained is reliable.

Low-Temperature Fluorescence Spectroscopy. NLN fluorescence spectra at 77 K and FLN spectra ($S_1 \leftarrow S_0$ excitation) at 4.2 K were obtained using a Lambda Physik FL-2002 dye laser pumped by a Lambda Physik Lextra 100 XeCl excimer laser as the excitation source. For FLN spectroscopy, several excitation wavelengths were used, each of which reveals a portion of the S_1 excited state vibrational frequencies of the

[2] K.-M. Li, E. L. Cavalieri, E. G. Rogan, M. George, M. L. Gross, and A. Seidel, Structure elucidation of the adducts formed by dibenzo-[*a*,*l*]pyrene diol epoxides with deoxyadenosine. *Chem. Res. Toxicol.*, accompanying paper.

[3] K. Roberts, C.-H. Lin, R. Jankowiak, and G. J. Small, On-line Identification of Diastereomeric Dibenzo[*a*,*l*]pyrene Diolepoxide-Derived Deoxyadenosine Adducts by Capillary Electrophoresis: Fluorescence Line-Narrowing and Non-Line Narrowing Spectroscopy. *J. Chromatogr. A*, in press.

Table 1. Calculated and Observed (0,0) Transition Energies, Dihedral Angles α and *β* with the Estimated Coupling Constants for the (*i,j*) Proton Pairs, and Structure Assignments for Various Conformations of *syn*- and *anti*-DB[*a,l*]P Tetrols[a]

DB[*a,l*]P tetrol	conformation	λ_{calc} (0,0) (nm)	λ_{obs}[c] (0,0) (nm)	α[d] (deg)	*β*[d] (deg)	structure assignment[f]	coupling constants[g]
trans-syn-	I[b]	381.4	382.2 (EtOH), 382.7 (g/w)	25	8	half-boat, pseudoaxial	vL/S/S
	II	384.0	387.0 (g/w)	−26	64	half-chair, pseudoequatorial	L/vL/vL
cis-syn-	I[b]	382.2	–	−24	62	half-chair, pseudoaxial	L/L/S
	II	384.5	385.2 (EtOH), 385.5 (g/w)	26	−60	half-chair, pseudoequatorial	S/S/S
trans-anti-	I[b]	383.2	383.6 (EtOH)	−24	60	half-chair, pseudoaxial	L/S/S
	II	384.4	385.4 (g/w)	27	−63	half-chair, pseudoequatorial	S/S/L
cis-anti-	I	382.0	382.8[e] (EtOH), 383.2 (g/w)	−24	−59	half-chair, pseudoaxial	S/S/S
	I′[b]	382.8	–	−24	−25	flattened, pseudoaxial	M/M/S
	II	384.3	–	−24	63	half-chair, pseudoequatorial	L/S/S

[a] Data from ref *26*. [b] These conformations were the most consistent with the room-temperature ^{1}H NMR data. [c] Spectroscopically observed (0,0) transition energies in ethanol (EtOH) or glycerol/water (g/w) at 77 K. [d] α describes the deviation from planarity in the fjord region, and *β* describes the conformation of the cyclohexenyl ring; see Figure 1. [e] The observed fluorescence (0,0) bands may correspond to either the I or the I′ conformation. [f] Conformation of the cyclohexenyl ring and orientation of the hydroxyl group at the C-14 position. [g] Estimated coupling constants for the (11,12), (12,13), and (13,14) proton pairs. L is large, vL very large, M medium, and S small; for details, see ref *26*.

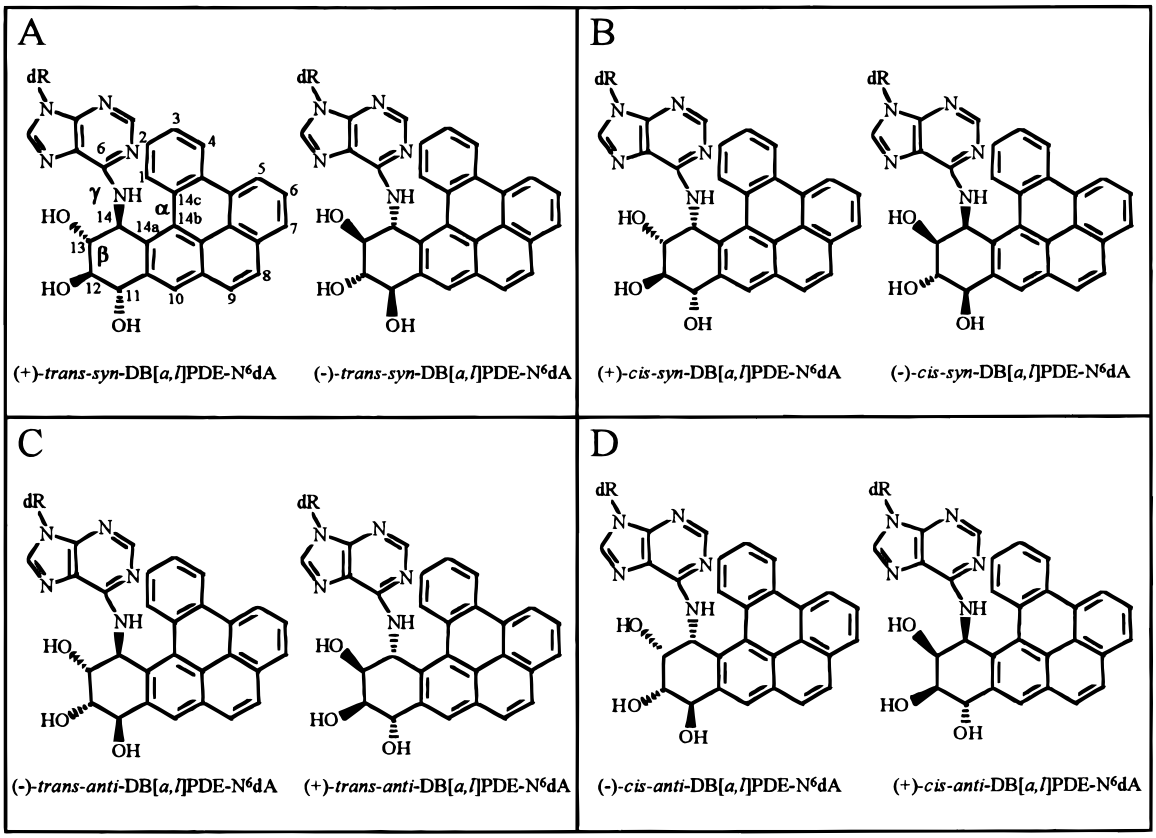

Figure 2. Molecular structures of the eight DB[*a,l*]PDE−14-N^{6}dA adducts that were investigated: (A) (±)-*trans-syn*-DB[*a,l*]PDE−14-N^{6}dA, (B) (±)-*cis-syn*-DB[*a,l*]PDE−14-N^{6}dA, (C) (±)-*trans-anti*-DB[*a,l*]PDE−14-N^{6}dA, and (D) (±)-*cis-anti*-DB[*a,l*] PDE−14-N^6-dA. The dihedral angles α, *β*, and *γ* will be used to describe the deviation from planarity in the fjord region, the conformation of the cyclohexenyl ring, and the orientation of the dA moiety, respectively. dR represents deoxyribose.

analyte (only selected spectra are presented). NLN spectra were obtained using nonselective excitation at 308 nm from the excimer laser. Samples were cooled in a glass cryostat with quartz optical windows. Fluorescence was dispersed by a McPherson 2061 1 m focal-length monochromator and detected by a Princeton Instruments IRY 1024/G/B intensified photodiode array. For time-resolved spectroscopy, a Princeton Instruments FG-100 pulse generator was employed; different detector delay times (0−60 ns) with a gate width of 200 ns were used. The resolution for FLN and NLN spectra was 0.05 and 0.8 nm, respectively. Two solvent matrices with different polarities were used: ethanol and a mixture of glycerol/water (50/50 v/v). Ethanol was spectrophotometric grade from Aldrich. Ultrapure grade glycerol was purchased from Spectrum Chemical (Gardena, CA). Samples (ca. 20 *μ*L) were transferred to quartz tubes (2 mm i.d.) and the tubes sealed with a rubber septum. Adduct concentrations were in the ∼10^{-6} M range.

Molecular Mechanics. Conformational analyses were carried out utilizing methods of molecular mechanics (MM), wherein energy calculations were performed with HyperChem's molecular modeling program (Release 5.1 for Windows Hypercube Inc.). HyperChem's force field (MM+) developed for organic molecules (*27*, *28*) was employed utilizing default parameters. As starting structures for the *trans-anti*-DB[*a,l*]PDE−14-N^{6}dA adduct, different model-built configurations in which the saturated ring was in either a half-chair or half-boat conformation were used. The Polak−Ribiere algorithm (in vacuo) was used for molecular mechanics optimization; the structures were

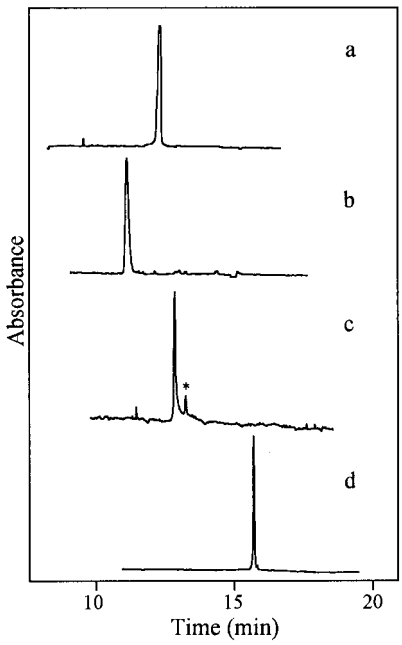

Figure 3. Room-temperature absorbance electropherograms acquired during CE separation of the HPLC-preseparated DB-[*a,l*]PDE-derived adduct standards: (a) (+)-*trans-syn*-DB[*a,l*]-PDE−N⁶dA, (b) (+)-*cis-syn*-DB[*a,l*]PDE−N⁶dA, (c) (−)-*trans-anti*-DB[*a,l*]PDE−N⁶dA, and (d) (−)-*cis-anti*-DB[*a,l*]PDE−N⁶dA. The asterisk denotes an impurity in the *trans-anti*-dA adduct.

refined until the rms gradient was less than 0.001 kcal/mol. Electrostatic contributions were evaluated by defining a set of bond dipole moments for polar bonds.

Molecular Dynamics (MD). To calculate thermodynamically favored conformations of the *trans-anti*-DB[*a,l*]PDE−14-N⁶dA adduct, separated from MM structures by energy barriers, quenched dynamics (simulated annealing) was used to explore the conformational space. No constraints were used during high-temperature searches of the conformational space. The starting half-chair and half-boat structures were minimized and then subjected to 50 ps of molecular dynamics at various temperatures between 300 and 400 K. Starting and final temperatures in a dynamic run were set to 0 K, and the heating and cooling times were set to 5 ps; the step size was 0.0005 ps. At various time points during the simulation, approximately 30 randomly selected structures were also annealed to 0 K and optimized. These optimized structures were subsequently used as starting points for further calculations. The two dihedral angles α and *β*, which define the distortion in the fjord region and the conformation of the cyclohexenyl ring (Figure 2), were used as variables during exploration of the conformational space. All simulations were performed in vacuo.

Results and Discussion

DB[*a,l*]PDE-derived dA adducts, which were isolated from reaction mixtures in which both the racemic mixture and the optically pure *syn*- and *anti*-DB[*a,l*]PDE were reacted with Ade, were studied. The NLN and FLN spectra obtained for adducts formed with the racemic mixtures of the respective diol epoxides gave four pairs of identical spectra (not shown) with the pairs corresponding to (+)- and (−)-enantiomers of *trans-syn-*, *cis-syn-*, *trans-anti-*, and *cis-anti*-DB[*a,l*]PDE−14-N⁶dA adducts. These identical fluorescence spectra for (+)- and (−)-enantiomers, for a given adduct, were expected since we have previously reported for benzo[*a*]pyrene diol epoxide-derived adducts that the (+)- and (−)-*trans* or (+)- and (−)-*cis* nucleoside enantiomers cannot be distinguished from one another by fluorescence methods (*23*). True (+)- and (−)-enatiomers cannot be distinguished since they are related by reflection (mirror) symmetry. Apparently, in the case of these DB[*a,l*]PDE−dA nucleotide adducts, the influence of the sugar moiety on the fluorescence characteristics is negligible. It is worthy to note that, due to the deoxyribose ring, these (+)- and (−)-dA adducts are not true enantiomers, but rather diastereomers.[2] In what follows, detailed characterization of dA adducts obtained with the optically pure (−)-*anti*-DB[*a,l*]PDE and (+)-*syn*-DB[*a,l*]PDE enantiomers will be discussed for both *trans*- and *cis*-opening dA adducts. Identical data for (+)-*anti*-DB[*a,l*]PDE and (−)-*syn*-DB[*a,l*]PDE enantiomers were also obtained (not shown).

NLN spectra of *trans-syn-*, *cis-syn-*, *trans-anti-*, and *cis-anti*-DB[*a,l*]PDE−14-N⁶dA adducts are shown in frames A−D of Figure 4, respectively. The major differences between the spectra in Figure 4 are revealed by the spectral position of the (0,0) bands, the intensity distribution of the vibronic bands, and the relative distribution of adduct conformations. The origin bands labeled as $(0,0)_I$ or $(0,0)_{II}$ indicate that they belong to different molecular conformations, vide infra. As was the case for *trans-anti-* and *trans-syn*-DB[*a,l*]P tetrol isomers (see Table 1), the NLN spectra of the dA adducts are also solvent-dependent. As a result, each of these adducts may exist in a conformation having its origin band at 382−385 nm (labeled as conformation I) and/or in a conformation having its origin band at ∼388−390 nm (denoted as conformation II) with the ratio of I/II being solvent-dependent. Additionally, variations in the vibronic intensity distribution and the S_0 vibrational frequencies (Figure 4) are not surprising given that the parent fluorophore B[*e*]P has C_{2V} symmetry, and the out-of-plane deformation, as well as the conformation of the cyclohexenyl ring, should depend on adduct stereochemistry as was observed in the case of the stereoisomeric DB-[*a,l*]P tetrols (*26*).

***syn*-DB[*a,l*]PDE−dA Adducts.** The NLN spectra of the (+)-*trans-syn*-DB[*a,l*]PDE−dA adduct, in ethanol (a) and glycerol/water (b) glass, are shown in Figure 4A. The spectra brought to light two fluorescence (0,0) bands at 382.0 and 389.0 nm with relative intensity distributions that are dependent on the solvent (see Table 2). Comparison with results obtained for the DB[*a,l*]P tetrols (see Table 1) and *trans-syn*-DB[*a,l*]PDE−14-N7Ade adducts (*24*) suggests that the main conformation of this adduct, with a characteristic origin band at 382.0 nm, has an open-like structure (conformer I) with the cyclohexenyl ring in a half-boat conformation. In the open-type structure, no strong interaction between dA and the aromatic system is possible. This is the dominant conformation observed in the ethanol matrix. In contrast, two distinct origin bands are observed in the glycerol/water matrix, which are assigned to conformer I [(0,0) band at 382.0 nm] and conformer II, respectively. The latter conformer has its origin band at 389.0 nm and an intense Herzberg−Teller origin band (*29*−*31*) at ∼760 cm^{-1}. On the basis of the results for the DB[*a,l*]P tetrols (see Table 1), and conformer II of *trans-syn*-DB[*a,l*]PDE−14-N7Ade (*24*), conformation II of *trans-syn*-DB[*a,l*]PDE−N⁶dA can be assigned as a half-chair with dA partially stacked over the distal ring in a folded-type configuration. This conformation is characterized by significant $\pi-\pi$ interaction between dA and the DB[*a,l*]P moiety, resulting in

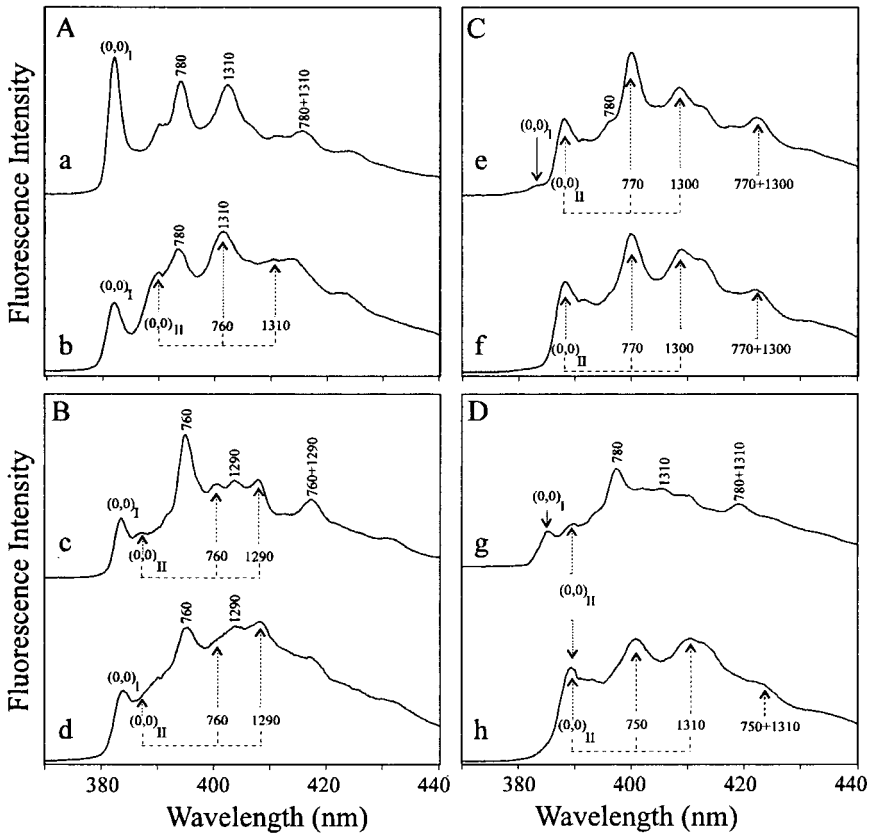

Figure 4. NLN fluorescence spectra obtained for (+)-*trans-syn*-DB[*a,l*]PDE−N^{6}dA (A), (+)-*cis-syn*-DB[*a,l*]PDE−N^{6}dA (B), (−)-*trans-anti*-DB[*a,l*]PDE−N^{6}dA (C), and (−)-*cis-anti*-DB[*a,l*]PDE−N^{6}dA (D) adducts in ethanol (spectra a, c, e, and g, respectively) and glycerol/water (spectra b, d, f, and h, respectively). $T = 77$ K. $\lambda_{ex} = 308$ nm. Delay time = 20 ns. Gate width = 200 ns. The numbers correspond to the ground state (S_0) vibrational frequencies.

Table 2. Fluorescence Characterization and Conformational Analysis of *syn*- and *anti*-DB[*a,l*]PDE−14-N^{6}dA Adducts

	ethanol		glycerol/water		assignment			
stereoisomeric dA adduct	(0,0) (nm)	conformation	(0,0) (nm)	conformation	α (deg)	β (deg)	conformation observed by ^{1}H NMR	cyclohexenyl ring, dA moiety[b]
(+)-*trans-syn*-	382.0	I[a]	382.0	I	positive	∼0	II	half-boat, pseudoaxial
	389.0	II	389.0	II	negative	positive		half-chair, pseudoequatorial
(+)-*cis-syn*-	383.6	I	384.0	I	negative	positive	I	half-chair, pseudoaxial
	388.0	II	388.0	II	positive	negative		half-chair, pseudoequatorial
(−)-*trans-anti*-	383.0[c]	I′	−	I′	28.5	−63.8	II′	half-chair, pseudoaxial ($\gamma = -158.4°$)
	388.1	**II′**	388.3	**II′**	30.9	59.0		half-chair, pseudoequatorial ($\gamma = -61.0°$)
(−)-*cis-anti*-	385.0	I	385.0[d]	I	positive	negative	II	half-chair, pseudoaxial
	389.0	II	389.0	II	negative	positive		half-chair, pseudoequatorial

[a] The bold Roman numerals denote the major conformations observed by low-temperature fluorescence. [b] Conformation of the cyclohexenyl (nonaromatic benzylic) ring and the orientation for the dA moiety; α, β, and γ are defined in Figure 1. [c] Minor conformation at the nucleoside level, but major conformation in single-stranded DNA (*16*) and in CE buffer solution.[2] In double-stranded DNA, this adduct adopts an intercalated conformation II (*16*) (see the text for details). [d] Very weak, so *cis-anti*-DB[*a,l*]PDE−14-N^{6}dA in glycerol/water glass exists mostly in conformer II (see Figures 4D and 10).

the red-shifted origin band. The NMR coupling constants obtained for the *trans-syn*-DB[*a,l*]PDE−dA adduct ($J_{11,12} \sim 7$ Hz, $J_{12,13} = 9.0$ Hz, and $J_{13,14} = 8.0$ Hz)[2] are consistent with the above half-chair assignment predicted by dynamical simulation for *trans-syn*-DB[*a,l*]P tetrol, for which the estimated coupling constants of the (11,12), (12,13), and (13,14) proton pairs were large, very large, and very large, respectively. We conclude, therefore, that *trans-syn*-DB[*a,l*]PDE−N^{6}dA, as observed in room-temperature NMR spectra (in Me_2SO solvent[2]), exists in folded-type conformation II.

The existence of the above-discussed conformers is confirmed by FLN spectra. Multiplet origin structures for the *trans-syn*-DB[*a,l*]PDE−14-N^{6}dA adduct in ethanol (spectra a and c) and in glycerol/water glass (spectra b and d) are shown in Figure 5. Frames A and B, which reveal different regions of the vibronic spectrum, show FLN spectra obtained for two different excitation wavelengths, 376.0 and 370.0 nm, respectively. The FLN bands [zero-phonon lines (ZPL)] are labeled with their S_1 vibrational frequencies in cm^{-1}. The vibrational frequencies of conformer I [$(0,0)_I \sim 382$ nm] are the same in both glasses, with minor differences in the intensity distribution due to larger inhomogeneous broadening commonly observed in a glycerol/water glass (*24*, *26*). However, comparison of the ZPL in spectra c and b of Figure 5 reveals significant differences in the vibrational frequencies between conformer I and II. For example, the

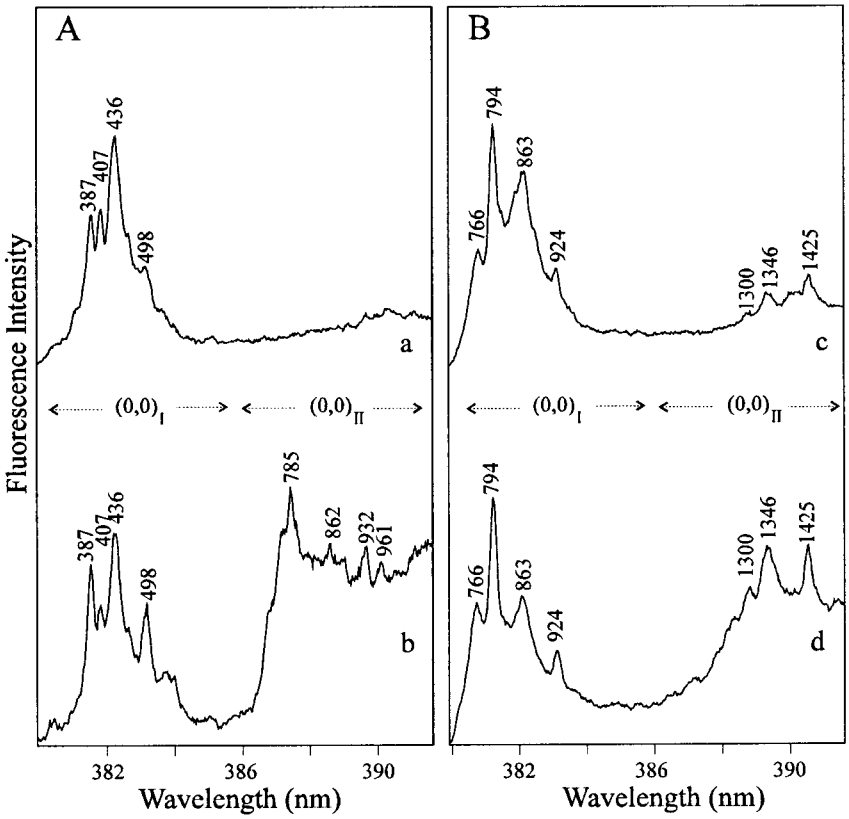

Figure 5. FLN spectra for (+)-*trans-syn*-DB[*a,l*]PDE−N⁶dA adducts in ethanol (spectra a and c) and 50/50 glycerol/water glass (spectra b and d) obtained for excitation wavelengths of 376.0 (A) and 370.0 nm (B), respectively. $T = 4.2$ K. The FLN peaks are labeled with their excited state vibrational frequencies, in cm^{-1}. The spectral range that is shown covers the fluorescence origin bands of conformations I and II (see the text).

excited state mode frequencies at 766, 794, 863, and 924 cm^{-1} are typical for conformer I, while modes at 785, 862, 932, and 961 cm^{-1} are observed for conformer II. These results suggest that the molecular conformations of conformer I and II are different. The same conclusion was reached on the basis of results presented in Figure 4A and calculations performed for *trans-syn*-DB[*a,l*]P tetrol (*26*), which indicate that the major conformation (conformer I) of the *trans-syn*-dA adduct has the cyclohexenyl ring in a half-boat structure. However, at room temperature the major conformation observed, as shown by ^{1}H NMR spectroscopy,[3] is conformation II with a half-chair structure for the cyclohexenyl ring, and a folded-type structure with dA in a pseudoequatorial position. The latter is consistent with the large experimentally observed red shift (∼470 cm^{-1}) of the $(0,0)_{II}$ band.

Frame B of Figure 4 shows NLN spectra of the (+)-*cis-syn*-DB[*a,l*]PDE−dA adduct in ethanol (curve c) and glycerol/water (curve d), respectively. In ethanol, the (0,0) band is located at 383.6 nm, while in glycerol/water, it is at 384 nm. The small spectral shift of 0.4 nm is due to the solvent effect. However, a small contribution from the red-shifted conformer II, with its origin band at ∼388 nm, is also revealed in both solvents. Unlike conformer I of *trans-syn*-DB[*a,l*]PDE−dA in ethanol, both conformations of the *cis* isomer have a weak (0,0) band and very intense Herzberg−Teller origin band at ∼760 cm^{-1}. The significant intensity of this band is attributed to electronic vibrational coupling between the S_1 and higher-energy dipole-allowed states, and is a consequence of the $S_1 \leftarrow S_0$ absorption transition being only weakly allowed (*31*).

For *cis-syn*-DB[*a,l*]P tetrol, only conformer I (*26*) was observed experimentally. However, modeling studies suggested that in vacuo *cis-syn*-DB[*a,l*]P tetrol may exist in two different half-chair conformations (*26*). Thus, on the basis of ref *26* and Table 1, the minor conformation of *cis-syn*-dA [conformer II having its (0,0) band at 388 nm] is tentatively assigned as a half-chair structure for the cyclohexenyl ring (negative β value) with dA in a folded-type geometry. The main conformation [conformer I with its (0,0) band at 384 nm] is assigned as a different half-chair (with a positive β value) and dA in an open-type configuration. The latter assignment is in good agreement with the ^{1}H NMR coupling constants for the proton pairs of the cyclohexenyl ring with $J_{11,12}$, $J_{12,13}$, and $J_{13,14}$ being ∼7 Hz (large), 7.5 Hz (large), and ∼3 Hz (small), respectively.[2]

In Figure 6, FLN spectra for the *cis-syn*-dA adduct, obtained with excitation at 378.0 nm, are presented. Spectra a and b were obtained in ethanol and glycerol/water glasses, respectively. Again, comparison of these spectra shows no differences in vibrational frequencies for conformer I [within the $(0,0)_I$ spectral range], proving that this conformation is the same in both glasses. The higher relative intensities of the 270 and 428 cm^{-1} modes in glycerol/water glass are, as in the case of the *trans-syn*-isomer, due to larger inhomogeneous broadening observed in glycerol/water glass. However, in glycerol/water, a relatively large contribution from adduct conformation II, having its origin band red-shifted to ∼389 nm, is also observed. This is in agreement with data presented in Figure 4B (spectrum d).

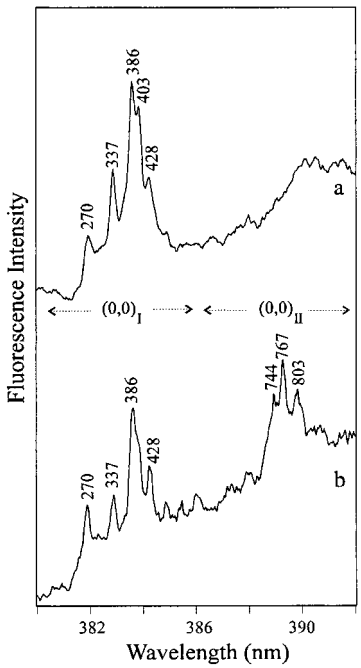

Figure 6. FLN spectra for (+)-*cis-syn*-DB[*a,l*]PDE−N^6dA adducts in ethanol (spectrum a) and 50/50 glycerol/water glass (spectrum b) obtained for an excitation wavelength of 378.0 nm. Delay time = 40 ns. T = 4.2 K. The $(0,0)_I$ and $(0,0)_{II}$ denote the origin bands of conformations I and II, respectively. The FLN peaks are labeled with their excited state vibrational frequencies, in cm^{-1}.

***anti*-DB[*a,l*]PDE−dA Adducts.** Frames C and D of Figure 4 show NLN fluorescence spectra for *trans-anti*- and *cis-anti*-DB[*a,l*]PDE−dA adducts. Spectra e and g and f and h were obtained in ethanol and glycerol/water glasses, respectively. In contrast to the *syn*-DB[*a,l*]PDE-derived adducts, the red-shifted conformation is clearly observed for both *trans-anti*- and *cis-anti*-dA adducts. Figure 4C shows that the major conformer for *trans-anti*-DB[*a,l*]PDE−dA, in both solvents, has its origin band at ∼389 nm. Also, in this case, the Herzberg−Teller origin band at ∼770 cm^{-1} is the most intense. The coupling constants previously calculated for conformer I (with a large $J_{11,12}$, a small $J_{12,13}$, and a small $J_{13,14}$) and conformer II (with a small $J_{11,12}$, a small $J_{12,13}$, and a large $J_{13,14}$) of *trans-anti*-DB[*a,l*]P tetrol (*26*) cannot explain the proton NMR coupling constants measured for the (+)-*trans-anti*-dA adduct, which are as follows: $J_{11,12}$ = 8.0 Hz (large), $J_{12,13}$ = 6.0 Hz (medium), and $J_{13,14}$ = 5.0 Hz (medium).[2] The $J_{12,13}$ and $J_{13,14}$ coupling constants for the (−)-*trans-anti*-dA adduct were not well resolved in Me_2-SO, and thus cannot be directly compared with those of (+)-*trans-anti*-dA. Nonetheless, we emphasize that circular dichroism,[3] NLN, and FLN spectra for (+)- and (−)-diastereomers were identical (data not shown), proving that the (+)- and (−)-*trans-anti*-DB[*a,l*]PDE−14-N7Ade adducts do exist in the same conformation.

To interpret the above data for *trans-anti*-DB[*a,l*]-PDE−14-N7Ade adducts, a theoretical investigation was initiated using MM and MD simulations. The minimum energy of the major conformation observed in MD simulations was 33.4 kcal/mol. Its structure is shown in Figure 7, which indicates that this adduct exists in a folded-type conformation. The dihedral angles α and β are both positive, with values of 30.9 and 59°, respectively. Angle α, defined as $C^{14a}-C^{14b}-C^{14c}-C^{1}$, describes a propeller-like distortion of the DB[*a,l*]P moiety that relieves the

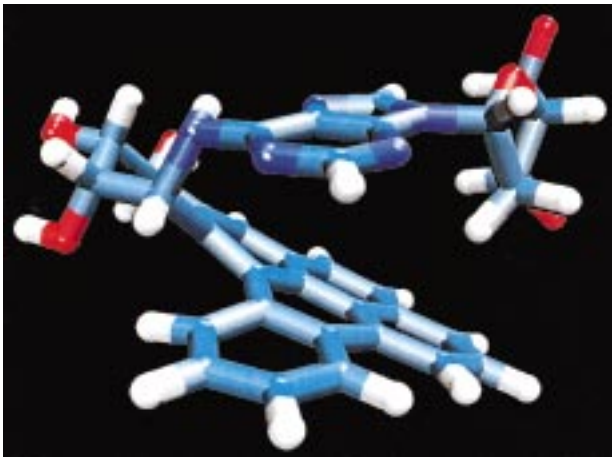

Figure 7. Optimized 0 K ground state structure of the *trans-anti*-DB[*a,l*]PDE−N^6dA adduct (conformation II′) obtained after simulated annealing and subsequent geometry optimization.

strain of the sterically hindered fjord region of the DB-[*a,l*]P residue by minimizing the steric repulsion between the H1 and H14 protons. Similar values of α were observed for *trans-syn*-DB[*a,l*]PDE−14-N7Ade (*24*) and benzo[*c*]phenanthrene diol epoxide adducts (*32*). On the other hand, the α and β values for *trans-anti*-DB[*a,l*]P tetrol, as shown in Table 1, are −24 and 60°, and 27 and −63° for conformers I, and II, respectively (*26*). The torsion angle γ ($C^6-N-C^{14}-C^{14a}$), which defines the relative orientation of the dA moiety, is equal to −61°. The half-chair structure of the cyclohexenyl ring, with dA at C14 in a semiaxial position, allows formation of a folded-type configuration with strong $\pi-\pi$ interaction between dA and the distal ring of DB[*a,l*]P (in the fjord region). This interaction is responsible for the spectroscopically observed red shift of the (0,0) band to ∼389 nm. The calculated coupling constants for the proton pairs $J_{11,12}$, $J_{12,13}$, and $J_{13,14}$ are large, medium, and medium, respectively, consistent with the ^{1}H NMR data.[2] Thus, the major conformation of the *trans-anti*-DB[*a,l*]-PDE−dA adduct, due to specific steric hindrance created by the fjord region of DB[*a,l*]P, exists in a conformation with positive α and β values, and is termed conformer II′ (Table 2).

Another unique conformation of *trans-anti*-dA (with a similar local energy minimum of ∼34 kcal/mol) was also observed in the simulations. In this conformation, the α and β values are 28 and −63.7° with the dA moiety in a pseudoaxial position, respectively, thus leading to the open-type structure with a large γ value of 158.4°. Consequently, no significant interaction between dA and the aromatic system is possible. We associate this structure with the experimentally observed minor conformer (I′) having its origin band at 383.0 nm. Although this conformer is hardly observed in ethanol (see Figure 4C), it is preferentially formed in a micellar CE buffer matrix.[2] The FLN spectra obtained for the *trans-anti*-dA isomer are shown in Figure 8; frames A and B were obtained for two different excitation wavelengths, 374.0 and 378.0 nm, respectively. Comparison of spectra a and c (ethanol) with spectra b and d (glycerol/water) indicates that the major, red-shifted, conformer II′ is the same in both glasses. The weak modes at 422, 549, and 627 cm^{-1} (spectrum a) correspond to the minor conformer I′ with its origin band at 383.0 nm.

The NLN spectra for the *cis-anti*-DB[*a,l*]PDE−dA adduct (Figure 4D), in contrast to those for *cis-anti*-DB-

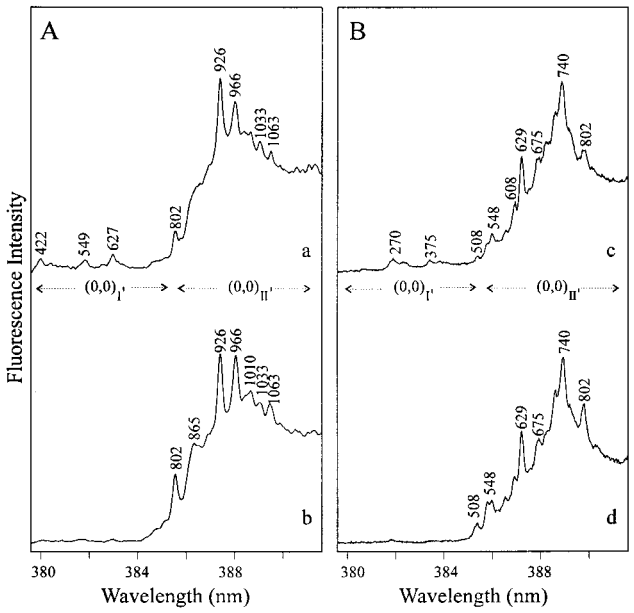

Figure 8. FLN spectra for (−)-*trans-anti*-DB[*a,l*]PDE−N⁶dA adducts in ethanol (spectra a and c) and 50/50 glycerol/water glass (spectra b and d) obtained for excitation wavelengths of 374.0 (A) and 378.0 nm (B), respectively. $T = 4.2$ K. The FLN peaks are labeled with their excited state vibrational frequencies, in cm^{-1}. The spectral range that is shown covers the fluorescence origin bands of conformations I′ and II′. The peaks at 270, 375, 422, 549, and 627 cm^{-1} correspond to minor conformation I′ (see the text for details).

[*a,l*]P tetrol (*26*), imply that two conformers may exist in ethanol, while only one conformer is observed in the glycerol/water glass. The origin bands of these conformers are at 385.4 and 389.8 nm, respectively. Room-temperature NMR data obtained in Me_2SO revealed the presence of only one conformation with a large $J_{11,12}$, a small $J_{12,13}$, and an undetermined $J_{13,14}$.[3] These coupling constants, based on the calculations for *cis-anti*-DB[*a,l*]P tetrol (*26*) and preliminary data for the *cis-anti*-DB[*a,l*]-PDE−dA adduct (data not shown), are consistent with conformation II in which the cyclohexenyl ring adopts a half-chair structure with a positive value of the dihedral angle β. The blue-shifted conformation [(0,0) = 385.0 nm] most probably has a negative value of β with dA in an open-type configuration.

Time-resolved spectroscopy revealed the *cis-anti*-dA adducts in conformation I possess a different fluorescence lifetime compared to adducts in conformation II, so the fraction of adducts in conformation I can be resolved. The spectrum obtained as the difference between two delay times (60 and 20 ns) of the observation window is shown in Figure 9. This temporal difference spectrum reveals that the adducts in conformation I have a longer fluorescence lifetime. As a result, only the origin band at 385.0 nm and its corresponding vibronic progression are exposed. This is in contrast to spectrum g of Figure 4D, where both conformers and their vibronic modes are observed.

The FLN spectra in Figure 10 for the *cis-anti*-isomer also suggest the presence of two unique conformations, consistent with the data depicted in Figure 4D. Comparison of the vibrational frequencies (∼850−1100 cm^{-1}) in spectra b of Figures 8A and 10 showed that the red-shifted conformers of the *trans-anti*- and *cis-anti*-dA adducts have different vibrational frequencies (e.g., 926 and 966 cm^{-1} vs 929 and 960 cm^{-1}, respectively). This

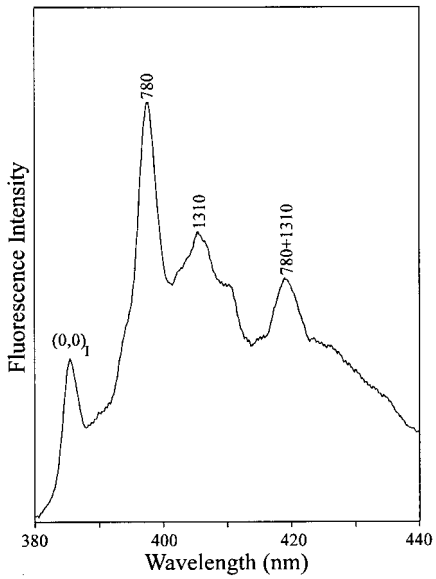

Figure 9. NLN fluorescence spectrum revealing the pure contribution from conformer I of the (−)-*cis-anti*-DB[*a,l*]PDE−N⁶dA adducts. The spectrum was obtained as a difference between the 60 and 20 ns delay times of the observation window. $\lambda_{ex} = 308$ nm. $T = 77$ K (see the text for details).

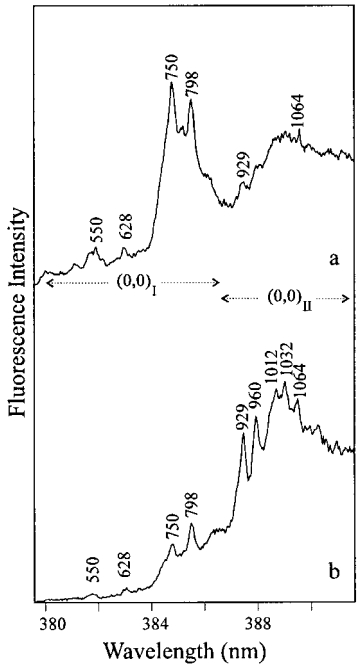

Figure 10. FLN spectra for (−)-*cis-anti*-DB[*a,l*]PDE−N⁶dA adducts in ethanol (spectrum a) and 50/50 glycerol/water glass (spectrum b) obtained for an excitation wavelength of 374.0 nm. Delay time = 40 ns. $T = 4.2$ K. In ethanol glass, the major conformation is I, while in glycerol/water glass, conformation II predominates. The FLN peaks are labeled with their excited state vibrational frequencies, in cm^{-1}.

supports our earlier assignment that conformer II′ of the *trans-anti*- and conformer II of the *cis-anti*-DB[*a,l*]PDE−N⁶dA isomers are clearly not the same.

Comparison of *trans-syn*- and *cis-syn*- versus *trans-anti*- and *cis-anti*-DB[*a,l*]PDE−N⁶dA adducts. Figure 11 shows four FLN spectra (in glycerol/water glass) obtained under identical conditions for *trans-syn*- (a), *cis-syn*- (b), *trans-anti*- (c), and *cis-anti*-DB[*a,l*]PDE−N⁶dA (d) diastereomers, respectively. These data show that the *syn*-type adducts (frame A), with ZPL at 387,

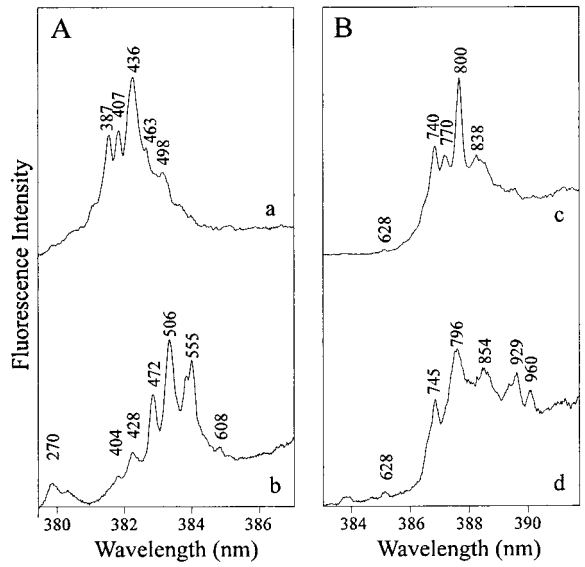

Figure 11. FLN spectra of *trans-syn-* (curve a), *cis-syn-* (curve b), *trans-anti-* (curve c), and *cis-anti*-DB[*a,l*]PDE−N^{6}dA adducts in a glycerol/water glass. T = 4.2 K. λ_{ex} = 376 nm. ZPL are labeled with their excited state vibrational frequencies, in cm^{-1}.

407, 436, 463, and 498 cm^{-1}, are indicative of *trans-syn*-dA adducts, while strong lines at 428, 472, 506, and 555 cm^{-1} are characteristic of the *cis-syn*-dA isomers. A different pattern of zero-phonon lines is observed in frame B for *trans-* and *cis-anti*-dA adducts, spectra c and d, respectively. Here the characteristic modes are 740, 770, 800, and 838 cm^{-1} for *trans-* and 745, 796, 854, 929, and 960 cm^{-1} for *cis-anti*-dA. Differences were also observed in other frequency regions (data not shown). With an experimental uncertainty of ±3 cm^{-1}, the observed variations are considered to be significant. These results show that *trans-* and *cis*-isomers of the *syn-* and *anti*-DB[*a,l*]PDE-derived dA adducts are readily distinguished by FLN spectroscopy.

Conclusions

We have demonstrated, using low-temperature fluorescence spectroscopy and computational chemistry, that not only the major but also the minor DB[*a,l*]PDE-derived dA adduct conformations can be characterized. Conformational data, including the results from molecular modeling and solvent-dependent studies performed for the diastereomeric DB[*a,l*]PDE−N^{6}dA adducts, provided insight into possible conformations of the cyclohexenyl ring and the orientation of the deoxyadenosine moiety. It was shown that both open-type (I and I′) and folded-type structures (II and II′) could be formed. Comparison of the fluorescence origin bands (Table 2) reveals that in a glycerol/water glass *trans-syn-* and *cis-syn*-dA isomers adopt mostly conformation I, while *trans-anti-* and *cis-anti*-dA isomers exist mostly in conformations II′ and II, respectively. The major low-temperature conformations of *cis-syn-* (I), *trans-anti-* (II′), and *cis-anti*-dA (II) observed by fluorescence are compatible with the ^{1}H NMR data. However, for *trans-syn*-DB[*a,l*]PDE−N^{6}dA, the ^{1}H NMR data show only conformer II, while the low-temperature fluorescence results show a mixture of conformers I (major) and II (minor).

The major conformers observed for *trans-anti*-dA (II′) and *cis-anti*-dA (II) are assigned as folded-type configurations with the same structure for the cyclohexenyl ring (positive β), opposite signs of α, and dA in a pseudoequatorial position partially stacked over the distal ring (see Table 2). The stacking leads to the experimentally observed red shift of the fluorescence origin bands. In contrast, the minor conformations of the above two isomers (I′ and I) are characterized by a different half-chair (negative β) with the dA moiety in a pseudoaxial position. Both minor conformers appear to exhibit similar deviation from planarity in the fjord region (positive α), as shown in Table 2. In contrast to the *trans-anti-* and *cis-anti*-DB[*a,l*]PDE−N^{6}dA adducts, where the major conformations have a half-chair structure in the cyclohexenyl ring, conformers I and II of *trans-syn*-dA feature half-boat and half-chair structures, respectively, with different orientations of the dA moiety. The *cis-syn*-dA adduct with the half-chair cyclohexenyl ring in conformers I (open) and II (folded), and α and β being positive and negative and negative and positive, respectively, is in agreement with the *cis-syn*-DB[*a,l*]P tetrol calculations (*26*). The different vibrational patterns in the FLN spectra can provide a means of distinguishing the *trans-* and *cis*-isomers for both *syn-* and *anti*-DB[*a,l*]PDE−14-N^{6}dA adducts. It is anticipated that these high-resolution FLN spectra will prove useful for future identifications of DB[*a,l*]PDE−DNA adducts (at the dAMP level) formed in biological systems.[4]

These fluorescence results establish that *anti*-DB[*a,l*]-PDE-derived dA adducts, the major adducts formed in mouse skin and calf thymus DNA (*16*), preferentially adopt conformation II (or II′) with origin bands at ∼388−390 nm. The large red shift of the (0,0) band is in agreement with modeling studies, which indicate that these conformers exist in a folded-type geometry with significant $\pi-\pi$ interactions. This suggests that molecular conformations of dA adducts may be important for understanding the preference of the bound metabolite toward external, base-stacked, and intercalated conformations, which were recently observed in DNA (*16*, *25*). Specifically, it was shown that in mouse skin the majority of *anti*-DB[*a,l*]PDE-derived DNA adducts adopt intercalated conformations, which in turn may influence their recognition by repair enzymes (*25*, *33*). The analysis of mouse skin DNA exposed to DB[*a,l*]P, which showed that external adducts are repaired more efficiently than intercalated adducts (*16*), accentuates the importance of adduct conformation. The conformational data presented in this paper suggest the majority of *anti*-DB[*a,l*]PDE−14-N^{6}dA adducts, due to a folded-type configuration, may be easily accommodated by the double helix of DNA. Moreover, the fact that the *anti*-dA adducts assume a folded-type configuration is consistent with the significant red shift of the fluorescence origin band of intercalated *anti*-DB[*a,l*]PDE−dA adducts observed for intact DNA (*16*). Therefore, we conclude that the large shifts (to ∼398 nm) of the fluorescence origin bands of DNA adducts observed in ref *16* are caused by type II (or II′) conformers, which allow intercalation and, as a result, strong $\pi-\pi$ interactions between the adduct and the DNA bases. In addition, it was shown here that the *cis-anti*-DB[*a,l*]PDE−14-N^{6}dA adduct forms an open-type structure (I), implying that this adduct adopts an external conformation with intact DNA, consistent with our

[4] P. Devanesan, F. Ariese, R. Jankowiak, G. J. Small, E. G. Rogan, and E. Cavalieri, A novel method for the isolation and identification of stable DNA adducts formed by dibenzo[*a,l*]pyrene and dibenzo[*a,l*]-pyrene 11,12-dihydrodiol 13,14-epoxides in vitro. *Chem. Res. Toxicol.*, accompanying paper.

earlier findings (*16*). Hence, it is entirely possible that the diverse structural conformations formed by DB[*a*,*l*]-PDE-derived DNA adducts are responsible for the high carcinogenic potency of DB[*a*,*l*]P.

Acknowledgment. Ames Laboratory is operated for the U.S. Department of Energy by Iowa State University under Contract W-7405-Eng-82. This research was supported by the National Institutes of Health (Grant POI CA49210-0). Partial support to R.J. and G.J.S. was provided by the Office of Health and Environmental Research, Office of Energy Research. We thank Dr. A. Seidel for providing the optically pure *syn*- and *anti*-DB-[*a*,*l*]P diol epoxides, Dr. E. L. Cavalieri for providing adduct standards, and Dr. F. Ariese for experimental help in the initial stage of this project.

References

(1) Cavalieri, E. L., Higginbotham, S., RamaKrishna, N. V. S., Devanesan, P. D., Todorovic, R., Rogan, E. G., and Salmasi, S. (1991) Comparative dose−response tumorigenicity studies of dibenzo[*a*,*l*]pyrene versus 7,12-dimethylbenz[*a*]anthracene, benzo-[*a*]pyrene, and two dibenzo[*a*,*l*]pyrene dihydrodiols in mouse skin and rat mammary gland. *Carcinogenesis* **12**, 1939−1944.

(2) Higginbotham, S., RamaKrishna, N. V. S., Johansson, S. L., Rogan, E. G., and Cavalieri, E. L. (1993) Tumor-initiating activity and carcinogenicity of dibenzo[*a*,*l*]pyrene versus 7,12-dimethylbenz[*a*]anthracene and benzo[*a*]pyrene at low dose in mouse skin. *Carcinogenesis* **14**, 875−878.

(3) Kozin, I. S., Gooijer, C., and Velthorst, N. H. (1995) Direct determination of dibenzo[*a*,*l*]pyrene in crude extracts of environmental samples by laser-excited Shpol'skii spectroscopy. *Anal. Chem.* **67**, 1623−1626.

(4) Mumford, J. L., Li, X., Hu, F., Lu, X. B., and Chuang, J. C. (1995) Human exposure and dosimetry of polycyclic aromatic hydrocarbons in urine from Xuan Wei, China with high lung cancer mortality associated with exposure to unvented coal smoke. *Carcinogenesis* **16**, 3031−3036.

(5) de Ratt, W. K., Kooijman, S. A. L. M., and Gielen, J. W. J. (1987) Concentrations of polycyclic hydrocarbons in airborne particles in The Netherlands and their correlation with mutagenicity. *Sci. Total Environ.* **66**, 95−114.

(6) Li, K.-M., Todorovic, R., Rogan, E. G., Cavalieri, E. L., Ariese, F., Suh, M., Jankowiak, R., and Small, G. J. (1995) Identification and quantitation of dibenzo[*a*,*l*]pyrene-DNA adducts formed by rat liver microsomes *in vitro*: preponderance of depurinating adducts. *Biochemistry* **34**, 8043−8049.

(7) Cavalieri, E., and Rogan, E. (1998) Mechanism of Tumor Initiation by Polycyclic Aromatic Hydrocarbons in Mammals. In *The Handbook of Environmental Chemistry, Vol. 3, Part I, PAHs and Related Compounds* (Neilson, A. H., Ed.) Springer-Verlag, Berlin and Heidelberg, Germany.

(8) Jankowiak, R., and Small, G. J. (1998) Analysis of PAH-DNA Adducts-Fluorescence Line-Narrowing Spectroscopy. In *The Handbook of Environmental Chemistry, Vol. 3, Part I, PAHs and Related Compounds* (Neilson, A. H., Ed.) Springer-Verlag, Berlin and Heidelberg, Germany.

(9) Cavalieri, E. L., and Rogan, E. G. (1992) The approach to understanding aromatic hydrocarbon carcinogenesis. The central role of radical cations in metabolic activation. *Pharmacol. Ther.* **55**, 183−199.

(10) Ralston, S. L., Seidel, A., Luch, A., Platt, K. L., and Baird, W. M. (1995) Stereoselective activation of dibenzo[*a*,*l*]pyrene to (−)-*anti*-(11*R*,12*S*,13*S*,14*R*)- and (+)-*syn*-(11*S*,12*R*,13*S*,14*R*)-11,12-diol-13,14-epoxides which bind extensively to deoxyadenosine residues of DNA in the human mammary carcinoma cell line MCF-7. *Carcinogenesis* **16**, 2899−2907.

(11) Conney, A. H. (1982) Induction of microsomal enzymes by foreign chemicals and carcinogenesis by polycyclic aromatic compounds. *Cancer Res.* **42**, 4875−4910.

(12) Luch, A., Glatt, H., Platt, K. L., Oesch, F., and Seidel, A. (1994) Synthesis and mutagenicity of the diastereomeric fjord-region 11,-12-dihydrodiol 13,14-epoxides of dibenzo[*a*,*l*]pyrene. *Carcinogenesis* **15**, 2507−2516.

(13) Harvey, R. G. (1991) *Polycyclic Aromatic Hydrocarbons: Chemistry and Carcinogenicity*, Cambridge University Press, Cambridge, U.K.

(14) Ralston, S. L., Lau, H. H. S., Seidel, A., Luch, A., Platt, K. L., and Baird, W. M. (1994) The potent carcinogen dibenzo[*a*,*l*]pyrene is metabolically activated to fjord-region 11,12-diol 13,14-epoxides in human mammary carcinoma MCF-7 cell cultures. *Cancer Res.* **54**, 887−890.

(15) Li, K.-M., RamaKrishna, N. V. S., Padmavathi, N. S., Rogan, E. G., and Cavalieri, E. L. (1994) Synthesis and structure determination of the adducts of dibenzo[*a*,*l*]pyrene diol epoxides and deoxyadenosine and deoxyguanosine. *Polycyclic Aromat. Compd.* **6**, 207−213.

(16) Jankowiak, R., Ariese, F., Hewer, A., Luch, A., Zamzow, D., Hughes, N. C., Phillips, D., Seidel, A., Platt, K.-L., Oesch, F., and Small, G. J. (1998) Structure, Conformations, and Repair of DNA Adducts from Dibenzo[*a*,*l*]pyrene: ^{32}P-Postlabeling and Fluorescence Studies *Chem. Res. Toxicol.* **11**, 674−685.

(17) Jankowiak, R., and Small, G. J. (1991) Fluorescence line narrowing: a high-resolution window on DNA and protein damage from chemical carcinogens. *Chem. Res. Toxicol.* **4**, 256−269.

(18) Rogan, E. G., Devanesan, P. D., RamaKrishna, N. V. S., Higginbotham, S., Padmavathi, N. S., Chapman, K., Cavalieri, E. L., Jeong, H., Jankowiak, R., and Small, G. J. (1993) Identification and quantitation of benzo[*a*]pyrene-DNA adducts formed in mouse skin. *Chem. Res. Toxicol.* **6**, 356−363.

(19) Devanesan, P. D., RamaKrishna, N. V. S., Padmavathi, N. S., Higginbotham, S., Rogan, E. G., Cavalieri, E. L., Marsh, G. A., Jankowiak, R., and Small, G. J. (1993) Identification and quantitation of 7,12-dimethylbenz[*a*]anthracene-DNA adducts formed in mouse skin. *Chem. Res. Toxicol.* **6**, 364−371.

(20) Kok, S. J., Posthumus, R., Bakker, I., Gooijer, C., Brinkman, U. A. Th., and Velthorst, N. H. (1995) Identification of benzo[*a*]-pyrene tetrols by reversed-phase liquid chromatography coupled semi-on-line to fluorescence line-narrowing spectroscopy. *Anal. Chim. Acta* **303** 3−10.

(21) Marsh, G. A., Jankowiak, R., Suh, M., and Small, G. J. (1994) Sequence dependence of benzo[*a*]pyrene diol epoxide-DNA adduct conformer distribution: a study by laser-induced fluorescence/polyacrylamide gel electrophoresis. *Chem. Res. Toxicol.* **7**, 98−109.

(22) Suh, M., Jankowiak, R., Ariese, F., Mao, B., Geacintov, N. E., and Small, G. J. (1994) Flanking base effects on the structural conformation of the (+)-*trans*-*anti*-benzo[*a*]pyrene diolepoxide adduct to N^2-dG in sequence-defined oligonucleotides. *Carcinogenesis* **15**, 2891−2898.

(23) Suh, M., Ariese, F., Small, G. J., Jankowiak, R., Liu, T.-M., and Geacintov, N. E. (1995) Conformational studies of the (+)-*trans*-, (−)-*trans*-, (+)-*cis*-, and (−)-*cis* adducts of *anti*-benzo[*a*]pyrene diolepoxide to N^2-dG in duplex oligonucleotides using polyacrylamide gel electrophoresis and low-temperature fluorescence spectroscopy. *Biophys. Chem.* **56**, 281−296.

(24) Ariese, F., Small, G. J., and Jankowiak, R. (1996) Conformational studies of depurinating DNA adducts from *syn*-dibenzo[*a*,*l*]pyrene diolepoxide. *Carcinogenesis* **17**, 829−837.

(25) Suh, M., Ariese, F., Small, G. J., Jankowiak, R., Hewer, A., and Phillips, D. H. (1995) Formation and persistence of benzo[*a*]-pyrene-DNA adducts in mouse epidermis *in vivo*: importance of adduct conformation. *Carcinogenesis* **16**, 2561−2569.

(26) Jankowiak, R., Ariese, F., Zamzow, D., Luch, A., Kroth, H., Seidel, A., and Small, G. J. (1997) Conformational Studies of Stereoisomeric Tetrols Derived from *syn*- and *anti*-Dibenzo[*a*,*l*]pyrene Diol Epoxides. *Chem. Res. Toxicol.* **10**, 677−686.

(27) Burkert, U., and Allinger, N. L. (1982) Molecular mechanics. *ACS Monogr.* **177**.

(28) Allinger, N. L. (1977) Conformational analysis 130. MM2: a hydrocarbon force field utilizing V1 and V2 torsional terms. *J. Am. Chem. Soc.* **99**, 8127−8134.

(29) Brown, J. C. (1982) Ph.D. Thesis, Iowa State University, Ames, IA.

(30) Brown, J. C., Duncanson, J. A., and Small, G. J. (1980) Fluorescence line narrowing spectrometry in glasses for direct determination of polycyclic aromatic hydrocarbons in solvent-refined coal. *Anal. Chem.* **52**, 1711−1715.

(31) Herzberg, G. (1966) Molecular Spectra and Molecular Structure, III. *Electronic Spectra and Electronic Structure of Polyatomic Molecules*, Chapter II, van Nostrand and Reinhold Co., New York.

(32) Geacintov, N. E., Cosman, M., Hingerty, B. E., Amin, S., Broyde, S., and Patel, D. J. (1997) NMR Solution Structures of Stereoisomeric Covalent Polycyclic Aromatic Carcinogen-DNA Adducts: Principles, Patterns, and Diversity. *Chem. Res. Toxicol.* **10**, 112−146.

(33) Wei, D., Maher, V., and McCormick, J. J. (1995) Site-specific rates of excision repair of benzo[*a*]pyrene diol epoxide adducts in the hypoxanthine phosphoribosyl transferase gene of human fibroblasts: correlation with mutation spectra. *Proc. Natl. Acad. Sci. U.S.A.* **92**, 2204−2208.

TX980233S